

A Helmholtz Energy Equation of State for *cis*-1-Chloro-2,3,3,3-tetrafluoro-1-propene [R-1224yd(Z)]

Ryo Akasaka · Eric W. Lemmon

Received: date / Accepted: date

Abstract A fundamental equation of state expressed explicitly in the Helmholtz energy is presented for R-1224yd(Z), an environmentally friendly refrigerant for centrifugal chillers, high-temperature heat pumps, and organic Rankine cycles. The equation of state is based on consistent experimental data for

Ryo Akasaka

Department of Mechanical Engineering, Faculty of Science and Engineering, Kyushu Sangyo University, Fukuoka 8138503, Japan

Research Center for Next Generation Refrigerant Properties (NEXT-RP), International Institute for Carbon-Neutral Energy Research (WPI-I2CNER), Kyushu University, Fukuoka 8190395, Japan

E-mail: ryo-a@ip.kyusan-u.ac.jp

ORCID: 0000-0003-2641-6031

Eric W. Lemmon

Applied Chemicals and Materials Division, National Institute of Standards and Technology, Boulder, CO 80305, USA

E-mail: eric.lemmon@nist.gov

ORCID: 0000-0002-0974-0203

the critical parameters, vapor pressures, saturated liquid and vapor densities, (p, ρ, T) behavior, vapor-phase sound speeds, liquid-phase sound speeds, and ideal-gas isobaric heat capacities. The equation is valid at temperatures from the triple-point temperature (157.8 K) to 473 K and pressures up to 35 MPa. In the valid range, expected relative uncertainties ($k = 2$) of the equation are 0.04 % for vapor pressures, 0.1 % for saturated liquid densities, 2 % for saturated vapor densities, 0.05 % for liquid densities, 0.3 % for vapor densities, 0.02 % for vapor-phase sound speeds, and 0.04 % for liquid-phase sound speeds, except in the critical region, where more significant uncertainties of up to 2 % are sometimes observed in densities. The equation exhibits reasonable behavior in the critical and extrapolated regions; this is demonstrated by several plots of derived properties over wide ranges of temperature and pressure.

Keywords Density · Equation of state · Heat capacity · R-1224yd(Z) · Sound speed · Vapor pressure · Virial coefficient

1 Introduction

The substance *cis*-1-chloro-2,3,3,3-tetrafluoro-1-propene (CAS No. 111512-60-8), also known as R-1224yd(Z), is one of the environmentally friendly refrigerants with negligible ozone depletion potential (ODP) and ultra-low global warming potential (GWP), which are 0.00023 and 0.88 (100yr), respectively [1]. This novel refrigerant is classified into the safety group “A1” (no flame propagation and lower toxicity) according to the ANSI/ASHRAE safety classi-

fication [2]. Its non-flammability and preferable thermodynamic properties are suitable for a working fluid of large-scale centrifugal chillers or high-temperature heat pumps as an alternative to 1,1,1,3,3-pentafluoropropane (R-245fa) or 2,2-dichloro-1,1,1-trifluoroethane (R-123), and analytical and/or experimental studies were extensively performed [3–8]. In addition, for organic Rankin cycles (ORC) for the recovery of waste heat, performance analyses were also attempted from both theoretical and experimental aspects [9–11].

Akasaka et al. [12] developed the first fundamental equation of state for R-1224yd(Z) in 2017 based on early experimental data for the vapor pressure [13, 14], saturated liquid and vapor densities [13, 14], (p, ρ, T) behavior [13], vapor-phase sound speed [15], and ideal-gas isobaric heat capacity [15]. Since the equation of state is available in REFPROP version 10.0 [16], it was often employed in the studies mentioned above; however, the first equation sometimes calculates inaccurate values for the vapor pressure and liquid properties because some of the early experimental data to which the equation was fitted were obtained with a low-purity sample, and because the data were located at limited ranges of temperature and pressure.

After the first equation of state was published, precise measurements became available for liquid densities and liquid-phase sound speeds at higher pressures [17–21]. Vapor pressure data consistent with these liquid-phase data were also reported [22]. This work formulated a new fundamental equation of state for R-1224yd(Z) mainly based on these recently published experimental data. Compared to the first equation, the new equation of state can be

applied to more extensive ranges of temperature and pressure and calculates more reasonable values for the vapor pressure, liquid density, and liquid-phase sound speed. The following sections discuss the fundamental constants of R-1224yd(Z), ancillary equations for the saturation properties, the functional form of the new equation of state, and comparisons to experimental data. Demonstrative plots are also provided to confirm reasonable behavior of the equation in the critical and extrapolated regions. Finally, expected uncertainties in properties calculated with the equation of state are presented as the conclusions.

2 Fundamental Constants

Figure 1 shows the molecular structure of R-1224yd(Z). The presence of a carbon-carbon double bond in the molecule yields a relatively short atmospheric lifetime of 20 days [1]. Table 1 lists the fixed-point constants and other characteristic properties of R-1224yd(Z), which are values calculated from the equation of state developed in this work, except the molar mass M , molar gas constant R , critical temperature T_c , and triple-point temperature T_{tp} . Sakoda and Higashi [22] experimentally determined the critical temperature, density, and pressure as 428.69 ± 0.02 K, 535 ± 5 kg · m⁻³ (≈ 3.603 mol · dm⁻³), and 3.331 ± 3 MPa. This critical temperature was used as the reducing temperature for the equation of state. Generally, experimental critical densities involve larger uncertainties than those in critical temperatures due to the infinite compressibility at the critical point and the difficulty of reaching thermody-

dynamic equilibrium; therefore, this work used the experimental critical density of Sakoda and Higashi [22] as an initial value for the reducing density, which was then slightly adjusted within the range of their uncertainty while fitting of the equation of state. This yields better representations of densities and vapor pressures near the critical point. The resulting value for the critical density (reducing density) was $3.632 \text{ mol} \cdot \text{dm}^{-3}$. The final equation of state calculates the critical pressure as 3.334 MPa at 428.69 K and $3.632 \text{ mol} \cdot \text{dm}^{-3}$, which almost agrees with the experimental value of Sakoda and Higashi [22]. Tanaka and Akasaka [23] also reported experimental critical parameters as $428.82 \pm 0.03 \text{ K}$, $540.8 \pm 7 \text{ kg} \cdot \text{m}^{-3}$ ($\approx 3.642 \text{ mol} \cdot \text{dm}^{-3}$), and $3.327 \pm 7 \text{ MPa}$; they are similar to the values of Sakoda and Higashi [22]. Tomassetti et al. [24] measured the melting point of R-1224yd(Z) as 157.8 K, which is regarded in this work as the triple-point temperature and the lower temperature limit of the applicable range of the equation of state. The vapor pressure at the triple point is calculated as 0.00254 kPa from the final equation of state.

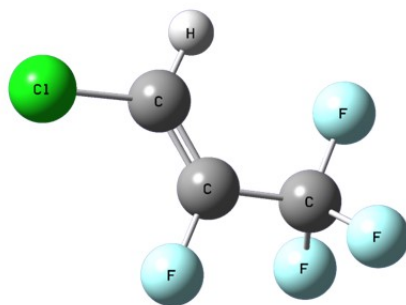


Fig. 1 Molecular structure of R-1224yd(Z) obtained from the geometry optimization with Gaussian 09 [25]

Table 1 Fixed-point constants and other characteristic properties of R-1224yd(Z)^a

Property	Symbol	Value	Unit
CAS number		111512-60-8	
Chemical formula		CF ₃ CF=CHCl (cis)	
Molar mass	M	148.4867	g · mol ⁻¹
Molar gas constant	R	8.314462618	J · mol ⁻¹ · K ⁻¹
Critical temperature	T_c	428.69	K
Critical pressure	p_c	3.334	MPa
Critical density	ρ_c	3.632	mol · dm ⁻³
Triple-point temperature	T_{tp}	157.8	K
Triple-point pressure	p_{tp}	0.00254	kPa
Saturated liquid density at triple point	ρ'_{tp}	11.49	mol · dm ⁻³
Saturated vapor density at triple point	ρ''_{tp}	1.933×10^{-6}	mol · dm ⁻³
Normal boiling point temperature	T_b	288.004	K
Saturated liquid density at normal boiling point	ρ'_b	9.344	mol · dm ⁻³
Saturated vapor density at normal boiling point	ρ''_b	0.04450	mol · dm ⁻³
Acentric factor	ω	0.3247	–
Reference temperature	T_0	273.15	K
Reference pressure	p_0	0.001	MPa
Ideal-gas enthalpy at reference state	h_0°	56255.100000	J · mol ⁻¹
Ideal-gas entropy at reference state	s_0°	278.76489776	J · mol ⁻¹ · K ⁻¹

^aAll properties in this table were determined in this work except M , R , T_c , and T_{tp} .

3 Ancillary Equations

Ancillary equations for the vapor pressure and saturated liquid and vapor densities were formulated based on values calculated from the equation of state. They provide rapid calculations of the saturation properties and also give excellent initial guesses for the iterative process to find rigorous solutions from the equation of state based on the Maxwell criterion. The equations presented here fulfill the requirements for the ancillary equations stated by Lemmon and Goodwin [26] and Gao et al. [27]. Coefficients N_i of each equation are given in Table 2.

The equation for the vapor pressure p_s is

$$\ln\left(\frac{p_s}{p_c}\right) = \frac{T_c}{T} (N_1\theta + N_2\theta^{1.5} + N_3\theta^{2.95} + N_4\theta^{5.8}), \quad (1)$$

where p_c is the critical pressure (3.334 MPa), T_c is the critical temperature (428.69 K), and $\theta = 1 - T/T_c$. Equation 1 is valid at temperatures from the triple point (157.8 K) to the critical temperature, and the average absolute deviation from the rigorous Maxwell solution is 0.0099 %. The saturated liquid and vapor densities (ρ' and ρ'') are calculated from the equations

$$\frac{\rho'}{\rho_c} = 1 + N_1\theta^{0.293} + N_2\theta^{0.332} + N_3\theta^{1.09} + N_4\theta^{1.55} + N_5\theta^{1.9} \quad (2)$$

and

$$\ln\left(\frac{\rho''}{\rho_c}\right) = N_1\theta^{0.23} + N_2\theta^{0.824} + N_3\theta^{2.72} + N_4\theta^6 + N_5\theta^{13}, \quad (3)$$

where ρ_c is the critical density (3.632 mol·dm⁻³). Equations 2 and 3 are applicable in the range from the triple-point temperature to the critical point temperature, and the average absolute deviations from the rigorous Maxwell solution are 0.0037 % in Eq. 2 and 0.0072 % in Eq. 3. Figure 2 shows relative deviations in values calculated with Eqs. 1, 2, and 3 versus temperature.

Table 2 Coefficients of Eqs. 1, 2, and 3

	Eq. 1	Eq. 2	Eq. 3
N_1	-7.5763	3.7298	-1.1894
N_2	1.5053	-2.6186	-6.3255
N_3	-3.7306	5.9922	-18.408
N_4	-2.7425	-10.250	-53.621
N_5		6.1004	-135.5

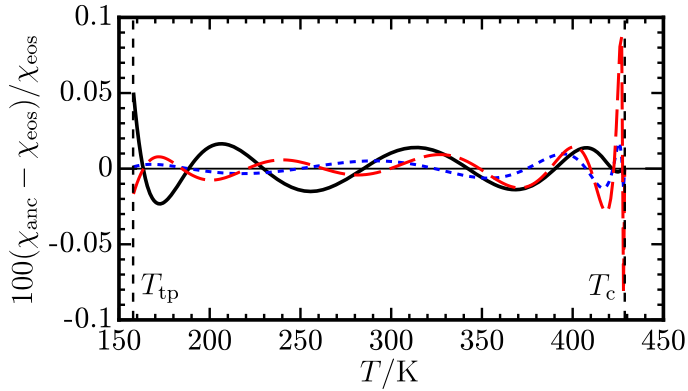


Fig. 2 Relative deviations in vapor pressures, saturated liquid densities, and saturated vapor densities calculated with the ancillary equations (χ_{anc}) from the Maxwell solution of the full equation of state (χ_{eos}): (black solid line) vapor pressure; (blue dotted line) saturated liquid density; (red dashed line) saturated vapor density.

4 Equation of State

The equation of state is expressed explicitly in the Helmholtz energy as the fundamental property with independent variables of temperature and density.

The equation has the form

$$\frac{a(T, \rho)}{RT} = \alpha(\tau, \delta) = \alpha^\circ(\tau, \delta) + \alpha^r(\tau, \delta), \quad (4)$$

where a is the molar Helmholtz energy, α is the dimensionless Helmholtz energy, R is the molar gas constant, $\tau = T_c/T$ is the reciprocal reduced temperature, and $\delta = \rho/\rho_c$ is the reduced density. The value of R used in this work is $8.314462618 \text{ J} \cdot \text{mol}^{-1} \cdot \text{K}^{-1}$ [28], which is a concise form of the exact value. The dimensionless Helmholtz energy α is split into an ideal-gas part α° representing ideal-gas properties and a residual part α^r corresponding to the influence of intermolecular forces between molecules.

The equation of state given by Eq. 4 is one of four fundamental forms in thermodynamics, and all thermodynamic properties in the single phase are calculated from derivatives of Eq. 4. Mathematical expressions for thermodynamic properties are presented in the literature [29,30]. The location of the saturation boundaries requires an iterative solution of the physical constraints on saturation (the Maxwell criteria). Kretzschmar et al. [31], Span [29], and Akasaka [32] discuss robust numerical algorithms to correctly obtain the Maxwell solutions.

4.1 Ideal-gas Helmholtz Energy

The ideal-gas Helmholtz energy a° is given by

$$a^\circ = h^\circ - pv - Ts^\circ = h^\circ - RT - Ts^\circ, \quad (5)$$

where h° and s° are the ideal-gas enthalpy and entropy expressed as

$$h^\circ(T) = h_0^\circ + \int_{T_0}^T c_p^\circ(T) dT \quad (6)$$

and

$$s^\circ(T, \rho) = s_0^\circ + \int_{T_0}^T \frac{c_p^\circ(T) - R}{T} dT - R \ln \left(\frac{\rho}{\rho_0} \right), \quad (7)$$

where c_p° is the ideal-gas isobaric heat capacity, T_0 is the temperature at the reference state (273.15 K), $\rho_0 = p_0/(RT_0)$ is the ideal-gas density at the reference state, p_0 is the reference state pressure (0.001 MPa), and h_0° and s_0° are the ideal-gas enthalpy and entropy at the reference state. Values for h_0° and s_0° are arbitrary, and this work determined them so that the specific enthalpy

and entropy of the saturated liquid state at 273.15 K are $200 \text{ kJ} \cdot \text{kg}^{-1}$ and $1 \text{ kJ} \cdot \text{kg}^{-1} \cdot \text{K}^{-1}$, corresponding to the common convention of the refrigeration industry. This was made after establishing the residual part. The final values for h_0° and s_0° are given in Table 1.

From Eqs. 5, 6, and 7, we obtain

$$\frac{a^\circ(T, \rho)}{RT} = \frac{h_0^\circ}{RT} - \frac{s_0^\circ}{R} - 1 + \frac{1}{RT} \int_{T_0}^T c_p^\circ(T) dT - \frac{1}{R} \int_{T_0}^T \frac{c_p^\circ(T) - R}{T} dT + R \ln \left(\frac{\rho}{\rho_0} \right) \quad (8)$$

or

$$\alpha^\circ(\tau, \delta) = \frac{h_0^\circ \tau}{RT_c} - \frac{s_0^\circ}{R} - 1 + \frac{1}{R} \int_{\tau_0}^{\tau} \frac{c_p^\circ}{\tau} d\tau - \frac{\tau}{R} \int_{\tau_0}^{\tau} \frac{c_p^\circ}{\tau^2} d\tau + \ln \left(\frac{\delta \tau_0}{\delta_0 \tau} \right), \quad (9)$$

where $\tau_0 = T_c/T_0$ and $\delta_0 = \rho_0/\rho_c$. Equation 9 indicates that the dimensionless ideal-gas Helmholtz energy α° can be analytically derived from an equation for the ideal-gas isobaric heat capacity. The rigid-rotor harmonic-oscillator (RRHO) approximation [33] is an approach to represent the ideal-gas heat capacities. For example, the ideal-gas isochoric heat capacity c_v° for nonlinear polyatomic molecules consisting of n atoms is given by

$$c_v^\circ = 3R + R \sum_{j=1}^{3n-6} \left(\frac{\Theta_j}{T} \right)^2 \frac{\exp(\Theta_j/T)}{[\exp(\Theta_j/T) - 1]^2}, \quad (10)$$

where Θ_j is the vibrational temperatures calculated from fundamental vibrational frequencies. In the right hand side, $3R$ arises from the translational and rotational contributions ($3/2R + 3/2R$), and the summation describes the vibrational contributions. Values of Θ_j can be estimated from spectroscopic data or quantum calculations; however, accurate and complete analyses for c_v°

according to Eq. 10 are generally limited to a few simple molecules such as diatomic and triatomic molecules. For polyatomic molecules, the RRHO approximation sometimes yields significant errors due to other additional effects, including the vibrational anharmonicity or the couplings between nuclear spin and molecular rotation, electronic and vibrational states, and vibrational and rotational states. Modifications of the RRHO model were attempted for relatively simple polyatomic molecules. For example, Pennington and Kobe [34] presented correction terms based on the first-order correction for the vibrational anharmonicity and rotation-vibration interaction. The correction terms were successfully employed for nitrous oxide. Tillner-Roth and Yokozeki [35] applied the correction terms of Pennington and Kobe [34] to difluoromethane (R-32) and formulated the ideal-gas Helmholtz energy of this refrigerant. For other polyatomic molecules, however, the complexity significantly increases in the application of the correction term. From a different viewpoint, Demenay et al. [36] introduced a scaling factor for Θ_j determined by fitting to experimental data of the ideal-gas heat capacity; however, this approach can be employed only for fluids for which experimental ideal-gas heat capacities are available.

In this work, the c_p° equation was empirically formulated based on the experimental data for the ideal-gas isobaric heat capacity and vapor-phase sound speed, following the recent fashion in the development of accurate equations of state. An initial equation consisting of several representative terms for vibrational contributions was roughly fitted to the experimental c_p° data of Kano et al. [15], and was further adjusted in the fitting of the residual part so that the

full equation of state represents experimental vapor-phase sound speeds [15] within their uncertainties. During the fitting, insignificant vibrational terms were removed, and terms with similar vibrational temperatures were combined into a single term. They were physically constrained so that the sum of coefficients would be close to the number of vibrational modes ($3n-6$) for non-linear polyatomic molecules. The final c_p° equation for R-1224yd(Z) is given by

$$\frac{c_p^\circ}{R} = n_0^\circ + \sum_{i=1}^2 n_i^\circ \left(\frac{m_i^\circ}{T}\right)^2 \frac{\exp(m_i^\circ/T)}{[\exp(m_i^\circ/T) - 1]^2}, \quad (11)$$

where the coefficients n_i° and exponents m_i° are shown in Table 3. Figure 3 shows c_p° values calculated from Eq. 11, as well as the experimental data [15]. Equation 11 represents the experimental data within their uncertainties. The ideal-gas Helmholtz energy derived from Eq. 11 is expressed as the form

$$\alpha^\circ(\tau, \delta) = \ln \delta + n_3^\circ + n_4^\circ \tau + (n_0^\circ - 1) \ln \tau + \sum_{i=1}^2 n_i^\circ \ln \left[1 - \exp\left(-\frac{m_i^\circ \tau}{T_c}\right) \right], \quad (12)$$

where the coefficients n_3° and n_4° are given in Table 3. The additional digits in these numbers are required to obtain the enthalpy and entropy values specified at the reference state.

Table 3 Coefficients and exponents of Eqs. 11 and 12 for R-1224yd(Z)

i	n_i°	m_i°
0	4.0	-
1	9.057	511
2	11.91	1425
3	-17.859290811	-
4	11.052900649	-

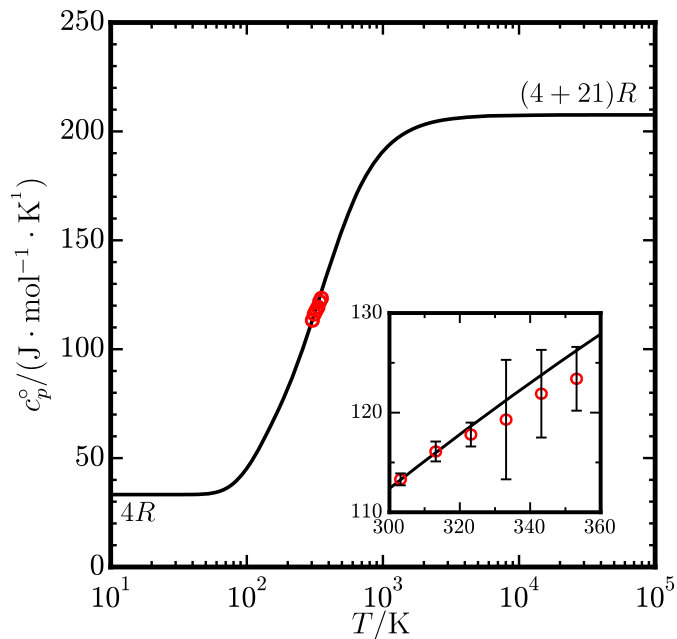


Fig. 3 Ideal-gas isobaric heat capacity c_p^o of R-1224yd(Z): (red \circ) Kano et al. [15]; (solid line) Eq. 11.

4.2 Residual Helmholtz Energy

While the ideal-gas Helmholtz energy can be derived analytically from the ideal-gas heat capacities, the residual Helmholtz energy must be empirically determined. This work employed the following functional form for the residual part:

$$\alpha^r(\tau, \delta) = \sum n_i \tau^{t_i} \delta^{d_i} + \sum n_i \tau^{t_i} \delta^{d_i} \exp(-\delta^{e_i}) + \sum n_i \tau^{t_i} \delta^{d_i} \exp[-\eta_i(\delta - \varepsilon_i)^2 - \beta_i(\tau - \gamma_i)^2], \quad (13)$$

where the first, second, and final summations are called polynomial, exponential, and Gaussian bell-shaped (simply Gaussian) terms, respectively. This form has often been used in the development of accurate equations of state

for industrial fluids. The number of terms, coefficients (n_i), exponents (t_i , d_i , and e_i), and Gaussian parameters (η_i , ε_i , β_i , and γ_i) are optimized by non-linear least-square fitting to experimental data under various thermodynamic constraints to ensure that the equation of state reasonably behaves in the critical and extrapolated regions. The algorithm for this procedure was originally developed by Lemmon and Jacobsen [30] and has been greatly extended by collaborations between correlators [27,37–42] over the last decade. Lemmon and Akasaka [43] and Akasaka and Lemmon [44] summarize the most recent fitting techniques. Akasaka and Lemmon [41] and Romeo and Lemmon [45] give examples of the thermodynamic constraints. As a starting point of the fitting, the residual part for R-1234yf [43] was used in this work, as done in the developments of the equations for R-1123 [42] and R-1132(E) [46]. During the fitting, two additional terms with higher temperature exponents were introduced to obtain reasonable effective inverse power law exponents (n_{eff}) [47] at temperatures below the critical temperature. The final form of the residual part for R-1224yd(Z) is given by

$$\alpha^r(\tau, \delta) = \sum_1^5 n_i \tau^{t_i} \delta^{d_i} + \sum_6^{12} n_i \tau^{t_i} \delta^{d_i} \exp(-\delta^{e_i}) + \sum_{13}^{19} n_i \tau^{t_i} \delta^{d_i} \exp[-\eta_i(\delta - \varepsilon_i)^2 - \beta_i(\tau - \gamma_i)^2], \quad (14)$$

where the coefficients, exponents, and Gaussian parameters are shown in Table 4. The 7th and 12th terms are those newly introduced in this work, and their effects are illustrated later.

Table 4 Coefficients and exponents of Eq. 14 for R-1224yd(Z)

i	n_i	t_i	d_i	e_i	η_i	β_i	γ_i	ε_i
1	0.05515868	1.0	4					
2	1.9416962	0.226	1					
3	-2.2385068	0.661	1					
4	-0.84144625	1.128	2					
5	0.22459576	0.51	3					
6	-1.6513724	1.98	1	2				
7	-0.022916841	8.5	1	3				
8	-1.588437	2.27	3	2				
9	0.56220803	0.89	2	1				
10	-0.67885338	2.78	2	2				
11	-0.027421084	1.0	7	1				
12	-0.021429988	6.36	2	3				
13	0.26924542	4.5	2		23.96	1028.	1.06	0.9578
14	-0.33022951	2.84	2		23.81	1014.	1.062	0.9577
15	2.2799188	1.15	1		1.327	1.23	1.296	0.8713
16	-0.42644754	1.25	1		1.941	1.146	1.245	1.183
17	-0.38611218	2.32	1		1.516	0.803	1.0	1.25
18	0.13232403	3.5	1		1.7	0.83	1.45	1.19
19	-0.33124629	1.06	1		2.23	1.21	1.215	0.842

5 Comparison to Experimental Data

Table 5 summarizes the experimental data currently available for R-1224yd(Z).

Figure 4 shows the distribution of the (p, ρ, T) and sound speed data on a p - T diagram, as well as the vapor pressure curve calculated from the equation of state. Although the equation of state was fitted only to selected experimental data, comparisons were made to all available data in Table 5, including those not used in the fitting. The quality of the fit is evaluated mainly by comparing expanded experimental uncertainties at the 95 % confidence interval (coverage factor $k = 2$) in experimental data to their average absolute deviations (AAD) from values calculated with the equation of state; the AAD is given by

$$\text{AAD}_\chi = \frac{100}{N_{\text{exp}}} \sum_{i=1}^{N_{\text{exp}}} \left| \frac{\chi_{i, \text{exp}} - \chi_{i, \text{calc}}}{\chi_{i, \text{exp}}} \right|, \quad (15)$$

where N_{exp} is the number of data points in a dataset, $\chi_{i,\text{exp}}$ is the i^{th} experimental value of a property χ , and $\chi_{i,\text{calc}}$ is the calculated value at the state conditions for $\chi_{i,\text{exp}}$. Table 5 gives the AAD_{χ} for each dataset. For comparison, the values from the first equation [12] are also given. Density deviations at their given temperatures and pressures are shown for the (p, ρ, T) data. For the vapor pressure, absolute differences in experimental data from calculated values ($|\chi_{i,\text{exp}} - \chi_{i,\text{calc}}|$) are sometimes evaluated.

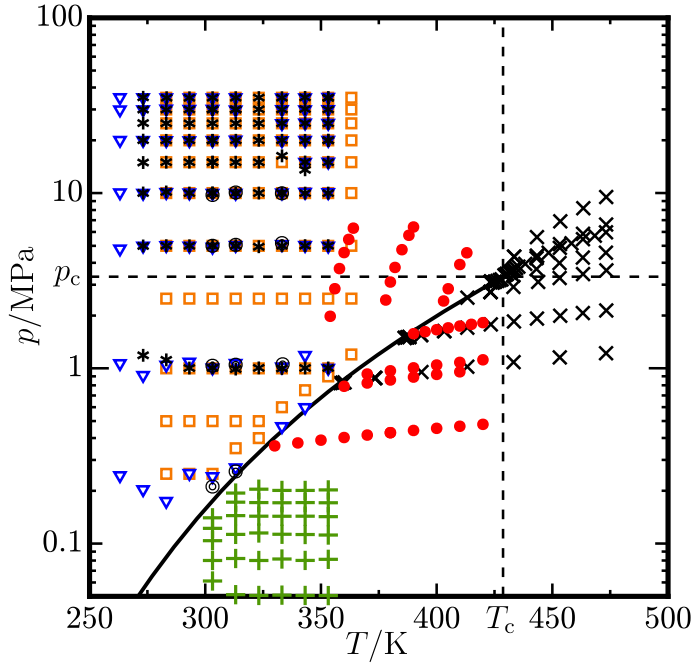


Fig. 4 Distribution of the experimental (p, ρ, T) and sound speed data of R-1224yd(Z). (p, ρ, T) data: (black \times) Fukushima et al. [13]; (red \bullet) Sakoda and Higashi [22]; (black $*$) Romeo et al. [18]; (orange \square) Fedele et al. [19]. Sound speed: (blue ∇) Lago et al. [17]; (green $+$) Kano et al. [15]; (black \odot) Nishiyama et al. [20].

Table 5 Available experimental data for the thermodynamic properties of R-1224yd(Z)

Author	Year	N	Purity (mass%)	Range		AAD (%)	
				T/K	p/MPa	First EOS [12]	This work
Vapor pressure							
Fukushima et al. [13]	2016	37	98.4	313–428		0.18	0.40
Higashi and Akasaka [14]	2016	24	99.5	310–425		0.31	0.46
Sakoda and Higashi [22]	2019	15	99.25 ^a	310–410		0.35	0.02
Raabe [48] ^b	2020	9	–	300–400		3.70	3.33
Bobbo et al. [49]	2020	31	99.25	293–353		0.41	0.88
Beltramino et al. [50]	2023	66	n.a.	274–338		0.45	0.26
Saturated liquid density							
Fukushima et al. [13]	2016	9 ^c	98.4	286–423		0.14	0.32
Higashi and Akasaka [14]	2016	5	99.5	409–428		1.60	1.75
Fedele et al. [19]	2020	9	99.25	283–363		0.04	0.03
Raabe [48] ^b	2020	9	–	300–400		1.07	1.05
Saturated vapor density							
Fukushima et al. [13]	2016	5 ^c	98.4	358–428		1.44	2.28
Higashi and Akasaka [14]	2016	6	99.5	424–428		3.29	1.50
Raabe [48] ^b	2020	9	–	300–400		7.94	7.42
(p, ρ, T) data							
Fukushima et al. [13]	2016	85	98.4	358–473	0.82–9.50	1.83	3.24
Sakoda and Higashi [22]	2019	46	99.25 ^a	330–420	0.36–6.41	0.15	0.17
Romeo et al. [18]	2019	80	99.25	273–353	0.99–35.1	0.03	0.07
Fedele et al. [19]	2020	94	99.25	283–363	1.00–35.0	0.05	0.02
Speed of sound							
Lago et al. [17]	2018	67	99.25	263–353	0.20–35.2	0.59	0.02
Kano et al. [15]	2020	36	99.85	303–353	0.04–0.20	0.01	0.01
Nishiyama et al. [20]	2021	11	n.a.	303–333	0.21–10.0	0.41	0.08
Isobaric heat capacity							
Fujiwara et al. [51]	2016	32	n.a.	278–323	0.48–0.51	0.81	1.59
Ideal-gas isobaric heat capacity							
Kano et al. [15]	2020	6	99.85	303–353		0.39	1.05

^aMole fraction^bMolecular simulation^cData in the vicinity of the critical point are excluded.

5.1 Saturation Properties

Five datasets are available for experimental vapor pressures of R-1224yd(Z).

Figure 5 shows relative deviations and differences in these data from values calculated with the equation of state. The data of Sakoda and Higashi [22], which are most consist with the (p, ρ, T) and sound speed data, are less scattered and accurately represented. The AAD in the data are 0.022 %, and all

data points are represented within their experimental uncertainty (1 kPa). The datasets of Higashi and Akasaka [14], Fukushima et al. [13], and Bobbo et al. [49] are less consistent with other experimental data, and they often show deviations larger than their experimental uncertainties. Although the data of Higashi and Akasaka [14] are reasonably represented at temperatures above 390 K, the deviations become gradually significant as temperature decreases. The deviation and difference at the lowest temperature (310 K) are 1.8 % and 4.0 kPa. Both the data of Fukushima et al. [13] and Bobbo et al. [49] show systematic positive deviations. The data of Fukushima et al. [13] always show deviations of around 0.5 %, and at temperatures above 400 K the differences exceed 10 kPa, which are off-scale in the figure. The data of Bobbo et al. [49] show more significant deviations than those of Fukushima et al., and the maximum difference is 5.3 kPa. The data of Beltramino et al. [50], published after the equation of state was established, are located at the lowest temperatures. They are consistent with the data of Sakoda and Higashi [22] at temperatures above 310 K. Deviations become larger at lower temperatures, but differences are always within 0.6 kPa, which is comparable to the experimental uncertainties.

Figure 6 shows the saturation boundary calculated from the equation of state on a T - ρ diagram, along with the experimental data for the saturated liquid and vapor densities [13, 14, 19]. The calculated saturation boundary reasonably expresses the experimental data. The rectilinear diameter (the mean value of the saturated liquid and vapor densities) is straight up to the critical

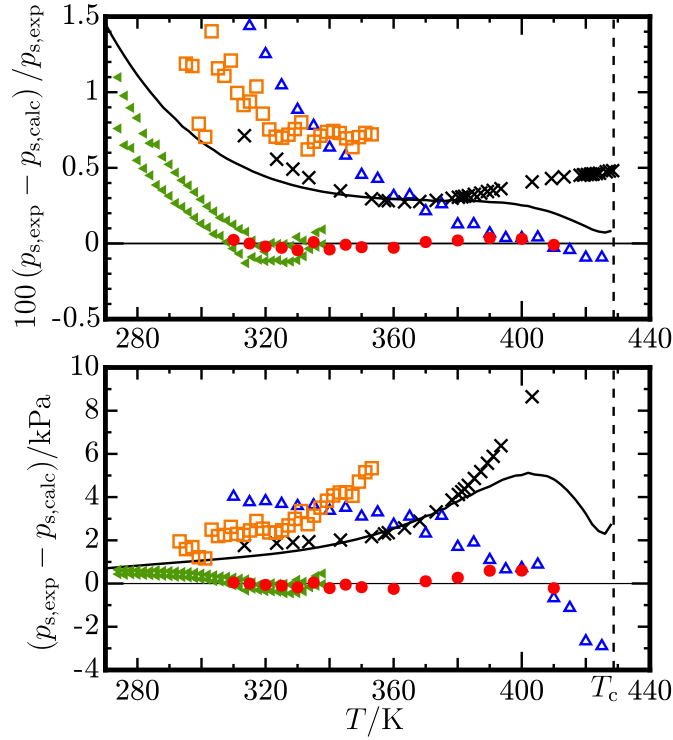


Fig. 5 Relative deviations (top panel) and differences (bottom panel) in the experimental vapor pressures of R-1224yd(Z) from values calculated with the equation of state: (black \times) Fukushima et al. [13]; (blue \triangle) Higashi and Akasaka [14]; (red \bullet) Sakoda and Higashi [22]; (orange \square) Bobbo et al. [49]; (green \blacktriangleleft) Beltramino et al. [50]; (solid line) Akasaka et al. [12] (first equation of state).

point, which is the physically correct behavior. Figure 7 shows relative deviations in the experimental data for the saturated liquid density. The data of Fedele et al. [19] are accurately represented; the AAD is 0.03 %, which is less than the experimental uncertainty in the density measurement (about 0.06 %). The data of Fukushima et al. [13] below 325 K agree with the equation, but data points above 420 K, probably including higher uncertainties, show larger deviations, which were excluded from the statistical analysis given in Table 5.

The data of Higashi and Akasaka [14] also include data points in the critical region, but they are represented reasonably.

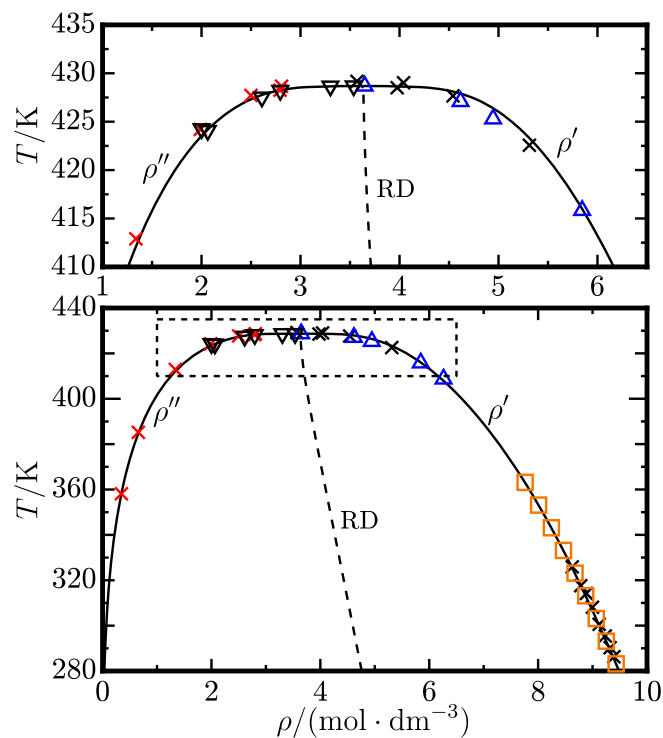


Fig. 6 Saturation boundary calculated from the equation of state (solid line) and experimental data for the saturated densities. Saturated liquid density: (black \times) Fukushima et al. [13]; (blue \triangle) Higashi and Akasaka [14]; (orange \square) Fedele et al. [19] Saturated vapor density: (red \times) Fukushima et al. [13]; (black ∇) Higashi and Akasaka [14]. The dashed line (RD) indicates the rectilinear diameter $(\rho' + \rho'')/2$.

5.2 (p, ρ, T) Data

Four datasets have been published for the (p, ρ, T) behavior of R-1224yd(Z).

Density deviations in these datasets from values calculated with the equation of state are shown in Fig. 8. The data of Fukushima et al. [13] are located in the vapor and supercritical regions. Deviations in the data are scattered due to low

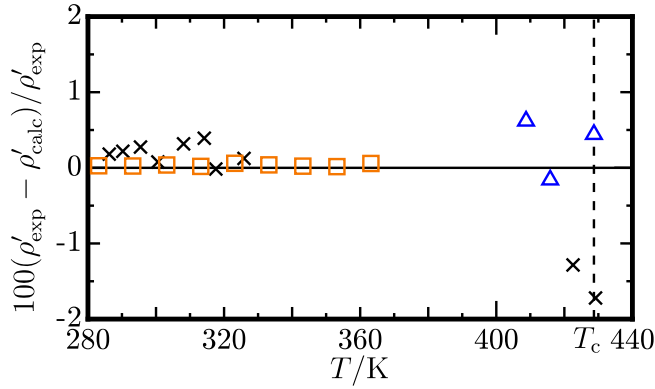


Fig. 7 Relative deviations in the experimental data for the saturated liquid density of R-1224yd(Z) from calculated values with the equation of state: (black \times) Fukushima et al. [13]; (blue \triangle) Higashi and Akasaka [14]; (orange \square) Fedele et al. [19].

sample purity, and some data points near the critical point show a significant deviation of over 10 %. The data of Sakoda and Higashi [22] include data points both in the vapor and liquid phases. The authors state that the experimental uncertainty in the density measurement is 0.15 %. Although the vapor data are slightly scattered, no systematic deviations are observed. The vapor, liquid, and overall AADs are 0.19 %, 0.12 %, and 0.17 %, respectively; they are similar to the experimental uncertainties. Figure 9 shows the second virial coefficient B derived from the vapor phase data of Sakoda and Higashi [22], as well as those calculated from the equation of state. The second virial coefficients from the equation are almost in accord with those from the experimental data.

The datasets of Romeo et al. [18] and Fedele et al. [19] are located in the liquid region at pressures up to 30 MPa, and they are accurately represented with the equation of state. Romeo et al. [18] first evaluated the experimental uncertainty in their density measurements as 0.05 %, and then it was revised to 0.044 % in their recent work [21]; this is sufficiently comparable to their

AAD (0.07 %). The experimental uncertainties in the data of Fedele et al. [19] are estimated to be between 0.01 % and 0.11 %, depending on temperature and pressure. The AAD in the data is 0.02 %, and all data points are represented within their uncertainties.

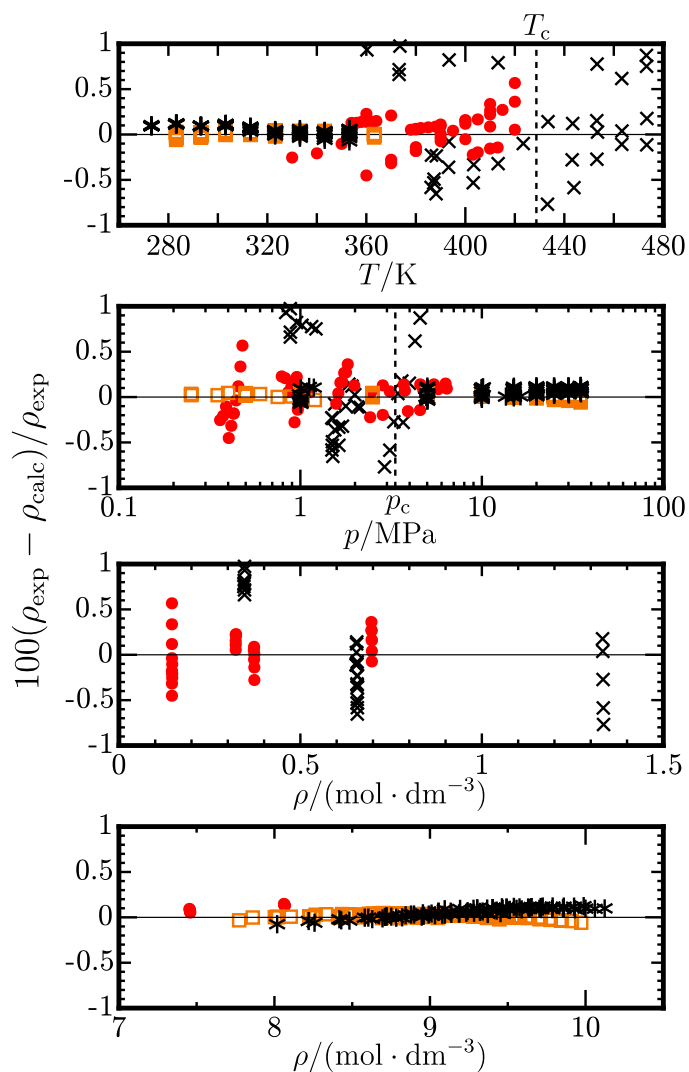


Fig. 8 Relative density deviations in the experimental (p, ρ, T) data from values calculated with the equation of state: (black \times) Fukushima et al. [13]; (red \bullet) Sakoda and Higashi [22]; (black $*$) Romeo et al. [18]; (orange \square) Fedele et al. [19].

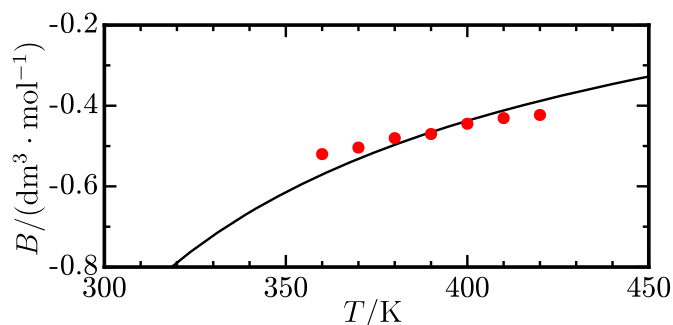


Fig. 9 Second virial coefficient B : (red \bullet) Derived from experimental vapor phase (p, ρ, T) data of Sakoda and Higashi [22]; (solid line) Calculated from the equation of state.

5.3 Caloric Data

For the sound speed of R-1224yd(Z), three datasets are available; one for the vapor phase and the others for the liquid phase. Deviations in these data are shown in Fig. 10. Overall, all datasets are mostly consistent with each other and are reasonably represented by the equation of state. Kano et al. [15] claim that a typical standard uncertainty in their vapor-phase sound speed data is $0.01 \text{ m} \cdot \text{s}^{-1}$; this corresponds approximately to a relative expanded uncertainty ($k = 2$) of 0.015 %, and a similar AAD (0.014 %) is observed in these data. All data points are represented within 0.08 %. The data of Lago et al. [17] for the liquid phase excellently agree with values calculated from the equation of state. The AAD in the data (0.02 %) is less than the relative expanded uncertainty (0.07 %) claimed by the authors, which was revised to 0.055 % in their recent work [21], and 93 % out of all data points are represented within this revised uncertainty. The data of Nishiyama et al. [20]

for the liquid phase are also represented well. Although Nishiyama et al. do not clearly mention the uncertainties in their data, the AAD (0.08 %) indicates a sufficient agreement. If two data points with deviations larger than 0.1 % are excluded, the AAD reduces to 0.05 %.

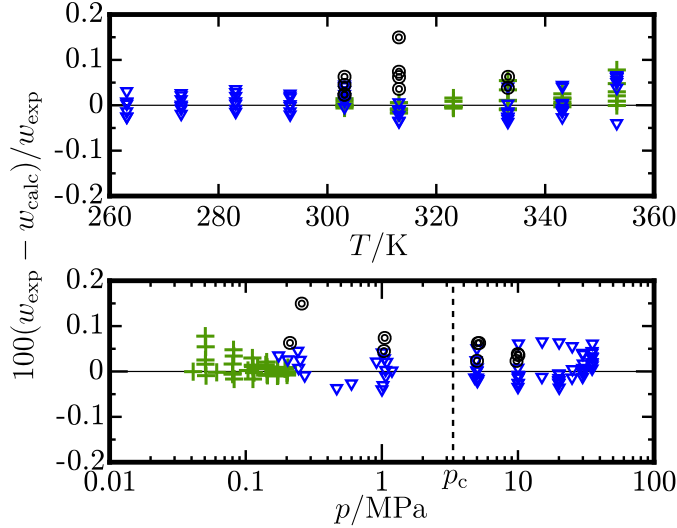


Fig. 10 Relative deviations in the experimental sound speed data from values calculated with the equation of state: (blue ∇) Lago et al. [17]; (green $+$) Kano et al. [15]; (black \odot) Nishiyama et al. [20].

Fujiwara et al. [51] measured liquid-phase isobaric heat capacities at 0.5 MPa. Figure 11 shows a plot of these heat capacity data on a c_p - T diagram along with the isobar calculated from the equation of state. The data show systematic negative deviations down to -3 %. The AAD in the data is 1.59 %, which exceeds the experimental uncertainties (0.35 % to 0.85 %); whether this is due to an experimental problem or is an artifact of the equation of state cannot be determined at this time.

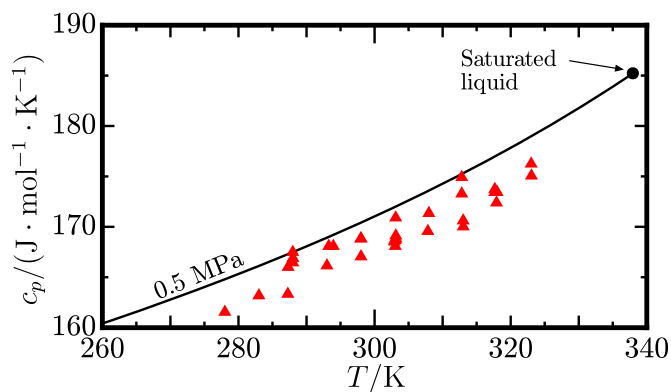


Fig. 11 Liquid-phase isobaric heat capacity at 0.5 MPa: (red \blacktriangle) Fujiwara et al. [51]; (solid line) Isobar calculated with the equation of state.

6 Behavior in the Critical and Extrapolated Regions

Derived properties calculated from higher-order derivatives of the Helmholtz energy are generally sensitive to underlying problems in equations of state, and therefore their plots on various thermodynamic coordinates are often used to verify the behavior of the equations in the critical and extrapolated regions; this is particularly essential for equations formulated from limited experimental data. The expected trends of derived properties, including virial coefficients, heat capacities, sound speeds, and ideal curves, were explained in other publications, for example, the work for R-125 [30] or propane [37]. Several plots generated from the equation of state for R-1224yd(Z) are demonstrated here.

6.1 Virial Coefficients

Virial coefficients are the most fundamental properties representing intermolecular forces between molecules in the vapor phase. Equations of state

must reasonably reproduce their correct behavior over a wide range of temperatures, even if no experimental data for the virial coefficients are available. In this work, the second, third, and fourth virial coefficients, which are related to the first, second, and third derivatives of the residual Helmholtz energy with respect to density, were consistently controlled during the fitting. Figure 12 shows trends in the virial coefficients obtained from the equation of state. These trends qualitatively correspond to those of the equation of state for the Lennard-Jones fluid [52]; B and C go to negative infinity at zero temperature, pass through zero at a moderate temperature, increase to a maximum, and asymptotically approach zero at extremely high temperatures. The theoretical trend in D is similar to those in B and C , except that a second maximum with a smaller magnitude appears at a higher temperature.

6.2 Heat Capacities and Sound Speeds

Derived properties related to the second partial derivatives of the Helmholtz energy are always monitored during the fitting and controlled so that they exhibit reasonable slope and curvature along isotherms, isobars, isochores, and the saturation lines.

The isochoric and isobaric heat capacities drastically change in the critical region and diverge to infinity at the critical point. Figure 13 shows the residual isochoric heat capacities c_v^r ($= c_v - c_v^o$) versus temperature along the saturation lines, isobars, and the critical isochore. This figure demonstrates reasonable behavior of the equation of state both in the critical and extrapo-

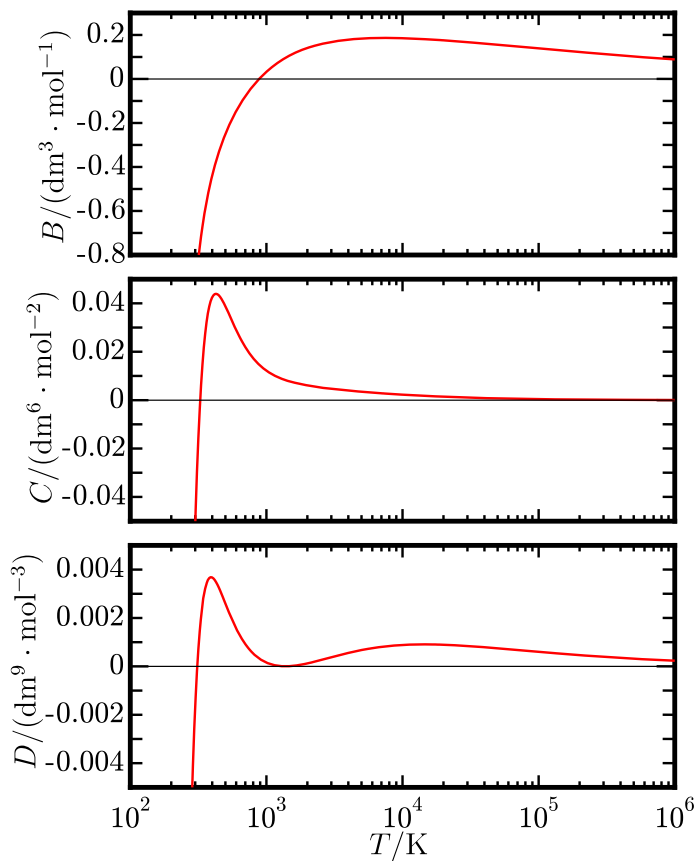


Fig. 12 Second, third, and fourth virial coefficients (B , C , and D) obtained from the equation of state.

lated regions. The critical isochore monotonically decreases from the critical point to higher temperatures, which means that temperature derivatives of the residual Helmholtz energy are properly formulated at $\delta = 1$ because the isochoric heat capacity is calculated only from the second partial derivative of the Helmholtz energy with respect to temperature.

In Fig. 14, sound speeds w are plotted versus temperature along isobars and saturation boundaries. There is no physically incorrect behavior in the isobars over wide temperature and pressure ranges. The saturated liquid line

should be a smooth arc when it is displayed on a logarithmic temperature scale; this can be confirmed in this figure.

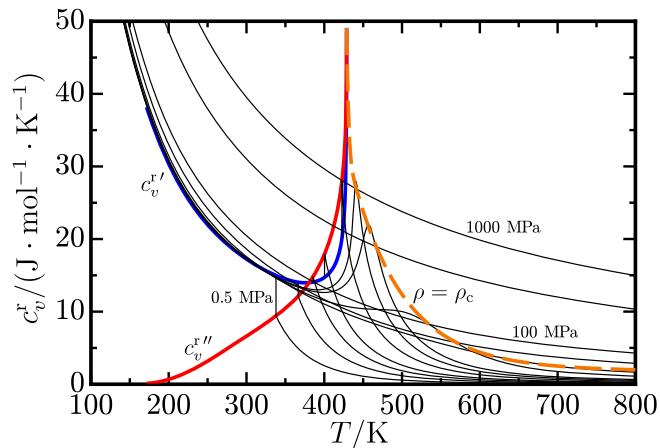


Fig. 13 Residual isochoric heat capacity (c_v^r) versus temperature along isobars at 0.5 MPa, 1 MPa, 1.5 MPa, 2 MPa, 3 MPa, 4 MPa, 5 MPa, 10 MPa, 20 MPa, 50 MPa, 100 MPa, 500 MPa, 1000 MPa, the saturation boundaries (blue and red lines), and the critical isochore ($\rho = \rho_c$) (dashed orange line).

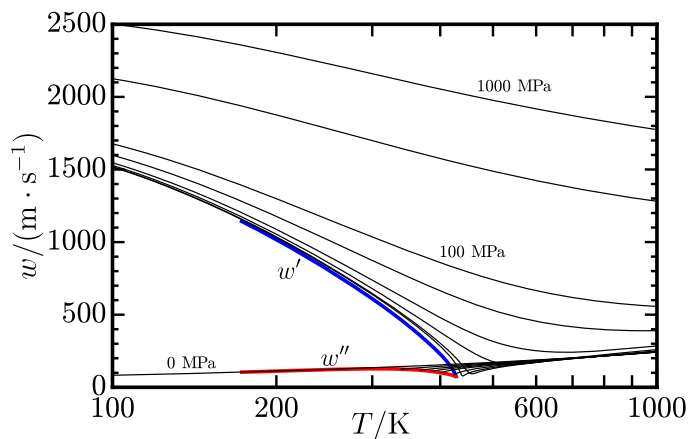


Fig. 14 Sound speed (w) versus temperature along isobars at 0.5 MPa, 1 MPa, 1.5 MPa, 2 MPa, 3 MPa, 4 MPa, 5 MPa, 10 MPa, 20 MPa, 50 MPa, 100 MPa, 500 MPa, 1000 MPa, and the saturation boundaries (blue and red lines).

6.3 Ideal Curves

Four characteristic curves (ideal curve, Boyle curve, Joule-Thomson inversion curve, and Joule inversion curve) are obtained from derivatives of the compressibility factor $Z = p/(\rho RT)$, as given in Table 6. Plots of these curves on a p - T diagram are often used to confirm the (p, ρ, T) behavior in extrapolated regions. The fitting process in this work verified the shapes of these curves, and if a physically incorrect bump was found along a curve, then the fitting process attempted to fix it by directly controlling its various derivatives. Figure 15 shows the four characteristic curves obtained from the equation of state. All curves exhibit smooth shapes in general, and no unnatural bumps are observed; this indicates that the equation of state would provide reasonable extrapolation of the (p, ρ, T) behavior.

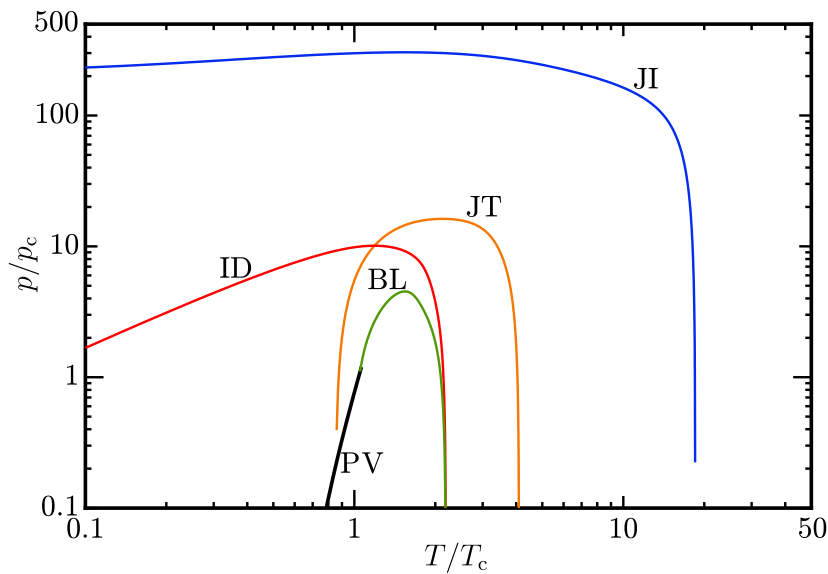


Fig. 15 Four characteristic curves and the vapor pressure curve (PV). ID: ideal curve; BL: Boyle curve; JT: Joule-Thomson inversion curve; JI: Joule inversion curve.

Table 6 Four characteristic curves.

Designation	Definition
Ideal curve	$Z = 1$
Boyle curve	$\left(\frac{\partial Z}{\partial \rho}\right)_T = 0$
Joule-Thomson inversion curve	$\left(\frac{\partial Z}{\partial T}\right)_p = 0$
Joule inversion curve	$\left(\frac{\partial Z}{\partial T}\right)_\rho = 0$

6.4 Phase Identification Parameter

The phase identification parameter (PIP), which is used to distinguish the location of a state point as being in the vapor phase or the liquid phase, highlights underlying problems in equations of states. The PIP is defined as

$$\text{PIP} = v \left[\frac{\frac{\partial^2 p}{\partial v \partial T}}{\left(\frac{\partial p}{\partial T}\right)_v} - \frac{\left(\frac{\partial^2 p}{\partial v^2}\right)_T}{\left(\frac{\partial p}{\partial v}\right)_T} \right] = 2 - \rho \left[\frac{\frac{\partial^2 p}{\partial \rho \partial T}}{\left(\frac{\partial p}{\partial T}\right)_\rho} - \frac{\left(\frac{\partial^2 p}{\partial \rho^2}\right)_T}{\left(\frac{\partial p}{\partial \rho}\right)_T} \right]. \quad (16)$$

If the PIP at a given condition is greater than 1, the state is the liquid phase, and if the PIP is less than 1, the state is the vapor phase. Figure 16 shows the PIP versus temperature along isobars from 0.1 to 1000 MPa, and Figure 17 displays the PIP versus density along isotherms from 100 to 5000 K. The isobars, isotherms, and saturation lines in these figures are smooth over wide ranges of temperature and density, and no unrealistic behavior is observed. In a PIP versus temperature plot, the saturated liquid line should have positive derivatives from low temperatures to the critical temperature and come up

to a very high value at the critical temperature; this can be observed from Fig. 16.

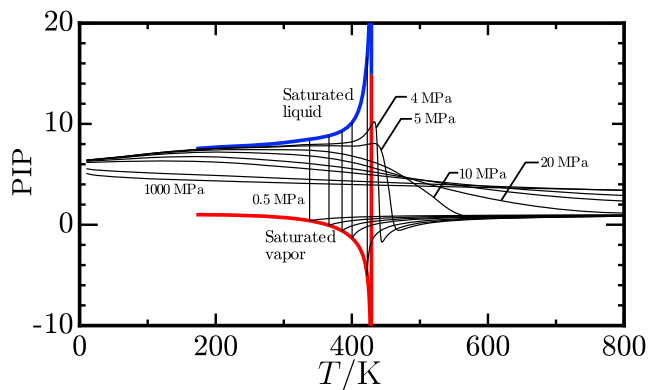


Fig. 16 Phase identification parameter (PIP) versus temperature along isobars at 0.5 MPa, 1 MPa, 1.5 MPa, 2 MPa, 3 MPa, 4 MPa, 5 MPa, 10 MPa, 20 MPa, 50 MPa, 100 MPa, 500 MPa, 1000 MPa, and the saturation boundaries (blue and red lines).

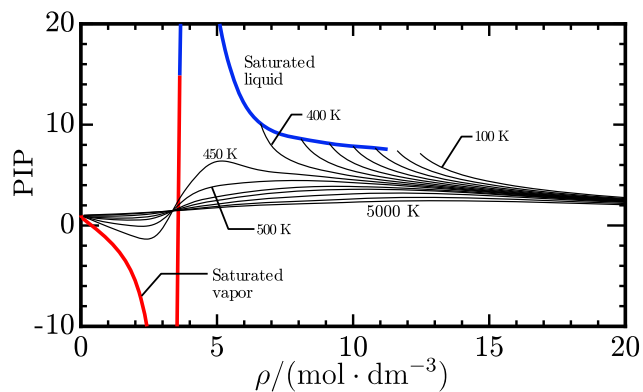


Fig. 17 Phase identification parameter (PIP) versus density along isotherms at 100 K, 150 K, 200 K, 250 K, 300 K, 350 K, 400 K, 450 K, 500 K, 600 K, 700 K, 1000 K, 2000 K, 5000 K, and the saturation boundaries (blue and red lines).

6.5 Effective Inverse Power Law Exponent

The effective inverse power law (IPL) exponent n_{eff} [47] expresses the relation between temperature and density along a constant residual entropy line. The definition of n_{eff} is

$$n_{\text{eff}} = 3 \left[\frac{\partial \ln(T)}{\partial \ln(\rho)} \right]_{s^r} = \frac{3\rho}{T} \left(\frac{\partial T}{\partial \rho} \right)_{s^r} = -\frac{3\rho}{T} \left(\frac{\partial s^r}{\partial \rho} \right)_T / \left(\frac{\partial s^r}{\partial T} \right)_\rho, \quad (17)$$

where s^r is the residual entropy given by

$$\frac{s^r}{R} = \tau \left(\frac{\partial \alpha^r}{\partial \tau} \right)_\delta - \alpha^r. \quad (18)$$

From Eqs. 17 and 18, we have

$$n_{\text{eff}} = \frac{3\delta(\tau\alpha_{\tau\delta}^r - \alpha_\delta^r)}{\tau^2\alpha_{\tau\tau}^r}, \quad (19)$$

where

$$\alpha_\delta^r = \left(\frac{\partial \alpha^r}{\partial \delta} \right)_\tau, \quad (20)$$

$$\alpha_{\tau\tau}^r = \left(\frac{\partial^2 \alpha^r}{\partial \tau^2} \right)_\delta, \quad (21)$$

and

$$\alpha_{\tau\delta}^r = \frac{\partial^2 \alpha^r}{\partial \tau \partial \delta}. \quad (22)$$

Bell [47] theoretically obtained the behavior of n_{eff} from the analysis of the second virial coefficients of the Lennard-Jones fluid; n_{eff} becomes zero approaching zero temperature, and after passing through a maximum, if asymptotically approaches approximately 12 at extremely high temperatures. Bell [47] also mentioned that a similar behavior is observed in fluids with the Stockmayer pair potential. In Fig. 18, n_{eff} values of dilute gases of R-1224yd(Z) and

R-1234yf are plotted versus temperature. For R-1224yd(Z), the equation of state developed in this work was used, and for R-1234yf, the equation developed by Lemmon and Akasaka [43] was employed. At temperatures higher than the critical temperatures, the trends in n_{eff} obtained from both equations are generally in accord with the expected behavior. At lower temperatures, however, a physically incorrect bump appears in the n_{eff} of R-1234yf. This bump is not observed in R-1224yd(Z), approaching asymptotically to zero; this is due to two additional terms introduced in the residual part of this work.

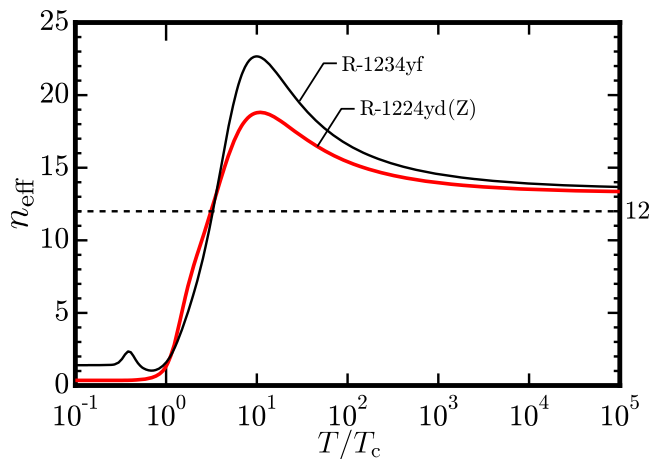


Fig. 18 Effective inverse power law exponent (n_{eff}) for dilute gases of R-1224yd(Z) and R-1234yf calculated with the equations of state.

7 Conclusions: Estimated Uncertainties of Calculated Properties

The fundamental equation of state expressed explicitly in Helmholtz energy was developed for R-1224yd(Z) from the consistent experimental datasets for the critical parameters, vapor pressure, saturated liquid and vapor densities,

(p, ρ, T) behavior, vapor-phase sound speed, liquid-phase sound speed, and ideal-gas isobaric heat capacity. The equation of state is valid at temperatures from the triple-point temperature (157.8 K) to 473 K and pressures up to 35.2 MPa. In the valid range, expected relative uncertainties ($k = 2$) of the equation are estimated as 0.04 % for vapor pressures, 0.1 % for saturated liquid densities, 2 % for saturated vapor densities, 0.05 % for liquid densities, 0.3 % for vapor densities, 0.02 % for vapor-phase sound speeds, and 0.04 % for liquid-phase sound speeds; they are almost double the average absolute deviations in the most consistent datasets. In the critical region, more significant uncertainties of up to 2 % are sometimes observed in densities. Plots of various derived properties show that the equation exhibits reasonable behavior in the critical and extrapolated regions.

As an aid in computer implementation, calculated property values from the equation of state are given in Table 7. Supporting Information provides a fluid file (R1224YDZ.FLD) for use in REFPROP [16] and TREND [53], a fluid file (R1224YDZ.json) for use in CoolProp [54], and Python code (R1224YDZ.py) to display the values in Table 7.

Table 7 Calculated property values from the equation of state for R-1224yd(Z) to verify computer code.[†]

T (K)	ρ (mol · dm ⁻³)	p (MPa)	c_v (J · mol ⁻¹ · K ⁻¹)	c_p (J · mol ⁻¹ · K ⁻¹)	w (m · s ⁻¹)
300	0	0	104.075	112.389	134.686
300	10	55.03325	122.878	160.984	892.196
300	0.05	0.1187058	108.960	120.269	129.430
400	8	21.17909	139.592	185.184	489.479
400	0.9	1.927264	145.150	212.723	103.907
430	4	3.418541	172.715	5047.06	67.4779

[†]All values were calculated with REFPROP DLL 10.0.0.98.

Acknowledgements The authors appreciate Ian H. Bell, National Institute of Standards and Technology, Boulder, for his generous support in programming the supplementary computer codes.

Declarations

Competing interests

The authors declare that they have no conflict of interest.

Authors' contributions

RA contributed to evaluating available experimental data, fitting the consistent data to the final equation, and writing, reviewing, and editing the whole manuscript. EWL contributed to establishing the fitting techniques for reliable equations of state and coding a computer program to implement it.

Funding

Partially funded by the National Institute of Standards and Technology

Availability of data and materials

not applicable

References

1. K. Tokuhashi, T. Uchimaru, K. Takizawa, S. Kondo, *J. Phys. Chem. A* **122**(12), 3120 (2018). DOI 10.1021/acs.jpca.7b11923
2. ANSI/ASHRAE Standard 34-2019; Designation and Safety Classification of Refrigerants (2019)
3. C. Mateu-Royo, J. Navarro-Esbrí, A. Mota-Babiloni, M. Amat-Albuixech, F. Molés, *Appl. Therm. Eng.* **152**, 762 (2019). DOI 10.1016/j.applthermaleng.2019.02.047

4. C. Arpagaus, S.S. Bertsch, in *Proceedings of IIR Rankine 2020 Conference-Advances in Cooling, Heating and Power Generation, 27-31 July, 2020, Online (Paper ID: 1129)* (2020)
5. K. Diewald, C. Arpagaus, B. Hebenstreit, in *Proceedings of IIR Rankine 2020 Conference-Advances in Cooling, Heating and Power Generation, 27-31 July, 2020, Online (Paper ID: 1166)* (2020)
6. S. Kujak, K. Schultz, E. Sorenson, in *Proceedings of IIR Rankine 2020 Conference-Advances in Cooling, Heating and Power Generation, 27-31 July, 2020, Online (Paper ID: 1118)* (2020)
7. C. Mateu-Royo, C. Arpagaus, A. Mota-Babiloni, J. Navarro-Esbrí, S.S. Bertsch, *Energy Convers. Manag.* **229**, 113752 (2021). DOI 10.1016/j.enconman.2020.113752
8. P. Giménez-Prades, J. Navarro-Esbrí, C. Arpagaus, A. Fernández-Moreno, A. Mota-Babiloni, *Renew. Sust. Energ. Rev.* **167**, 112549 (2022). DOI 10.1016/j.rser.2022.112549
9. J. Navarro-Esbrí, M. Amat-Albuixech, F. Molés, C. Mateu-Royo, A. Mota-Babiloni, R. Collado, *Energy* **193**, 116701 (2020). DOI 10.1016/j.energy.2019.116701
10. M. Amat-Albuixech, J. Navarro-Esbrí, F. Molés, A. Mota-Babiloni, C. Mateu-Royo, in *Proceedings of IIR Rankine 2020 Conference-Advances in Cooling, Heating and Power Generation, 27-31 July, 2020, Online (Paper ID: 1163)* (2020)
11. G. Righetti, G.A. Longo, S. Mancin, C. Zilio, in *Proceedings of IIR Rankine 2020 Conference-Advances in Cooling, Heating and Power Generation, 27-31 July, 2020, Online (Paper ID: 1209)* (2020)
12. R. Akasaka, M. Fukushima, E.W. Lemmon, in *Proceedings of 21st European Conference on Thermophysical Properties (Graz, Austria)* (2017)
13. M. Fukushima, H. Hayamizu, M. Hashimoto, in *Proceedings of 16th International Refrigeration and Air Conditioning Conference at Purdue (West Lafayette, IN, USA)* (2016)
14. Y. Higashi, R. Akasaka, in *Proceedings of the 11th Asian Thermophysical Properties Conference (Yokohama, Japan)* (2016)
15. Y. Kano, Y. Kayukawa, Y. Fujita, *Int. J. Refrig.* **118**(1), 354 (2020). DOI 10.1016/j.ijrefrig.2020.06.027

-
16. E.W. Lemmon, I.H. Bell, M.L. Huber, M.O. McLinden. NIST Standard Reference Database 23: Reference Fluid Thermodynamic and Transport Properties-REFPROP, Version 10.0, National Institute of Standards and Technology (2018). DOI 10.18434/T4/1502528. URL <https://www.nist.gov/srd/refprop>
 17. S. Lago, P.G. Albo, J.S. Brown, in *Proceedings of 20th Symposium on Thermophysical Properties (Boulder, CO, USA)* (2018)
 18. R. Romeo, S. Lago, P.A.G. Albo, in *Proceedings of the 12th Asian Thermophysical Properties Conference (Xi'an, China)* (2019)
 19. L. Fedele, S. Bobbo, M. Scattolini, C. Zilio, R. Akasaka, *Int. J. Refrig.* **118**(8), 139 (2020). DOI 10.1016/j.ijrefrig.2020.06.001
 20. T. Nishiyama, T. Kuranari, L. Gao, Y. Higashi, R. Akasaka, in *Proceedings of 21th Symposium on Thermophysical Properties (Boulder, CO, USA)* (2021)
 21. S. Lago, P.A.G. Albo, R. Akasaka, R. Romeo, submitted to *Int. J. Refrig.* (2023)
 22. N. Sakoda, Y. Higashi, *J. Chem. Eng. Data* **64**(9), 3983 (2019). DOI 10.1021/acs.jced.9b00374
 23. K. Tanaka, R. Akasaka, *Int. J. Refrig.* **131**, 61 (2021). DOI 10.1016/j.ijrefrig.2021.07.010
 24. S. Tomassetti, G. Di Nicola, C. Kondou, *Int. J. Refrig.* **133**, 172 (2022). DOI 10.1016/j.ijrefrig.2021.10.008
 25. M.J. Frisch, G.W. Trucks, H.B. Schlegel, G.E. Scuseria, M.A. Robb, J.R. Cheeseman, G. Scalmani, V. Barone, G.A. Petersson, H. Nakatsuji, X. Li, M. Caricato, A.V. Marenich, J. Bloino, B.G. Janesko, R. Gomperts, B. Mennucci, H.P. Hratchian, J.V. Ortiz, A.F. Izmaylov, J.L. Sonnenberg, D. Williams-Young, F. Ding, F. Lipparini, F. Egidi, J. Goings, B. Peng, A. Petrone, T. Henderson, D. Ranasinghe, V.G. Zakrzewski, J. Gao, N. Rega, G. Zheng, W. Liang, M. Hada, M. Ehara, K. Toyota, R. Fukuda, J. Hasegawa, M. Ishida, T. Nakajima, Y. Honda, O. Kitao, H. Nakai, T. Vreven, K. Throssell, J.A. Montgomery, Jr., J.E. Peralta, F. Ogliaro, M.J. Bearpark, J.J. Heyd, E.N. Brothers, K.N. Kudin, V.N. Staroverov, T.A. Keith, R. Kobayashi, J. Normand, K. Raghavachari, A.P. Rendell, J.C. Burant, S.S. Iyengar, J. Tomasi, M. Cossi, J.M. Millam, M. Klene,

-
- C. Adamo, R. Cammi, J.W. Ochterski, R.L. Martin, K. Morokuma, O. Farkas, J.B. Foresman, D.J. Fox. Gaussian 09 Revision D.01 (2013). Gaussian Inc. Wallingford CT
26. E.W. Lemmon, A.R.H. Goodwin, J. Phys. Chem. Ref. Data **29**(1), 1 (2000). DOI 10.1063/1.556054
27. K. Gao, J. Wu, P. Zhang, E.W. Lemmon, J. Chem. Eng. Data **61**(8), 2859 (2016). DOI 10.1021/acs.jced.6b00195
28. E. Tiesinga, P.J. Mohr, D.B. Newell, B.N. Taylor, J. Phys. Chem. Ref. Data **50**(3), 033105 (2021). DOI 10.1063/5.0064853
29. R. Span, *Multiparameter Equations of State: An Accurate Source of Thermodynamic Property Data* (Springer Berlin, 2000)
30. E.W. Lemmon, R. Jacobsen, J. Phys. Chem. Ref. Data **34**(1), 69 (2005). DOI 10.1063/1.1797813
31. H.J. Kretzschmar, T. Zschunke, J. Klinger, A.I. Dittman, *An Alternative Method for the Numerical Calculation of the Maxwell Criterion in Vapour Pressure Computations, Properties of Water And Steam: Proceedings of The 11th International Conference* (CRC Press, 1990)
32. R. Akasaka, J. Therm. Sci. Technol. **3**(3), 442 (2008). DOI 10.1299/jtst.3.442
33. D.A. McQuarrie, *Statistical Mechanics* (Harper & Row, 1975)
34. R.E. Pennington, K.A. Kobe, J. Chem. Phys. **22**(8), 1442 (1954). DOI 10.1063/1.1740413
35. R. Tillner-Roth, A. Yokozeki, J. Phys. Chem. Ref. Data **26**(6), 1273 (1997). DOI 10.1063/1.556002
36. A. Demenay, J. Glorian, P. Paricaud, L. Catoire, Int. J. Refrig. **79**, 207 (2017). DOI 10.1016/j.ijrefrig.2017.03.023. URL <http://dx.doi.org/10.1016/j.ijrefrig.2017.03.023>
37. E.W. Lemmon, M.O. McLinden, W. Wagner, J. Chem. Eng. Data **54**(12), 3141 (2009). DOI 10.1021/je900217v
38. M. Thol, E.W. Lemmon, R. Span, High Temp.-High Press. **41**(2), 81 (2012)
39. R. Akasaka, Y. Zhou, E.W. Lemmon, J. Phys. Chem. Ref. Data **44**(5), 013104 (2015). DOI 10.1063/1.4913493

-
40. S. Herrig, M. Thol, A.H. Harvey, E.W. Lemmon, *J. Phys. Chem. Ref. Data* **47**(5), 043102 (2018). DOI 10.1063/1.5053993
 41. R. Akasaka, E.W. Lemmon, *J. Chem. Eng. Data* **64**(11), 4679 (2019). DOI 10.1021/acs.jced.9b00007
 42. R. Akasaka, Y. Higashi, N. Sakoda, S. Fukuda, E.W. Lemmon, *Int. J. Refrig.* **119**(11), 457 (2020). DOI 10.1016/j.ijrefrig.2020.07.011
 43. E.W. Lemmon, R. Akasaka, *Int. J. Thermophys.* **43**(8), 119 (2022). DOI 10.1007/s10765-022-03015-y
 44. R. Akasaka, E.W. Lemmon, *J. Phys. Chem. Ref. Data* **51**(2), 023101 (2022). DOI 10.1063/5.0083026
 45. R. Romeo, E.W. Lemmon, *Int. J. Thermophys.* **43**(10), 146 (2022). DOI 10.1007/s10765-022-03059-0
 46. R. Akasaka, E.W. Lemmon, in *Proceedings of 2nd IIR Conference on HFOs and Low GWP blends, 16-18, June, 2021, Online (Paper ID: 1035)* (2021)
 47. I.H. Bell, *J. Chem. Phys.* **152**(16), 164508 (2020)
 48. G. Raabe, *J. Chem. Eng. Data* **65**(3), 1234 (2020). DOI 10.1021/acs.jced.9b00588
 49. S. Bobbo, A. Bet, M. Scattolini, L. Fedele, *J. Chem. Eng. Data* **65**(9), 4263 (2020). DOI 10.1021/acs.jced.0c00231
 50. G. Beltramino, L. Rosso, R. Cuccaro, V. Fericola, *Int. J. Refrig.* **145**, 90 (2023). DOI 10.1016/j.ijrefrig.2022.09.026
 51. N. Fujiwara, Y. Muto, H. Sato, in *Proceedings of the 2016 Symposium on Environmental Engineering (Kanawaza, Japan) (in Japanese)* (2016)
 52. M. Thol, G. Rutkai, A. Köster, R. Lustig, R. Span, J. Vrabec, *J. Phys. Chem. Ref. Data* **45**(2), 023101 (2016). DOI 10.1063/1.4945000
 53. R. Span, R. Beckmüller, S. Hielscher, A. Jäger, E. Mickoleit, T. Neumann, S. Pohl, B. Semrau, M. Thol. *TREND. Thermodynamic Reference and Engineering Data 5.0. Lehrstuhl für Thermodynamik, Ruhr-Universität Bochum.* (2020)
 54. I.H. Bell, J. Wronski, S. Quoilin, V. Lemort, *Ind. Eng. Chem. Res.* **53**(6), 2498 (2014). DOI 10.1021/ie4033999